arXiv:1203.6486v1 [cond-mat.str-el] 29 Mar 2012

Range separated hybrid exchange-correlation functional analyses of W and/or N(S) (co)doped anatase TiO_2

Veysel Çelik and Ersen Mete
Department of Physics, Balıkesir University, Balıkesir 10145, Turkey
(Dated: March 1, 2013)

Electronic properties and atomic structures of W, N, S, W/N, and W/S dopings of anatase TiO_2 have been systematically investigated using the density functional theory (DFT). The exchange and correlation effects have been treated with Heyd, Scuseria and Ernzerhof (HSE) hybrid functional. Mixing traditional semi-local and non-local screened Hartree-Fock (HF) exchange energies, the HSE method corrects the band gap and also improves the description of anion/cation derived gap states. Enhanced charge carrier dynamics, observed for W/N codoped titania, can partly be explained by the passivative modifications of N 2*p* and W 5*d* states on its electronic structure. Following this trend we have found an apparent band gap narrowing of 1.03 eV for W/S codoping. This is due to the large dispersion of S 3*p* states at the valance band (VB) top extending its edge to higher energies and Ti–S–W hybridized states appearing at the bottom of the conduction band (CB). W/S-TiO_2 might show strong visible light response comparable to W/N codoped anatase catalysts.

PACS numbers: 71.20.Nr, 71.55.-i, 61.72.Bb

I. INTRODUCTION

In the growing area of renewable energy, TiO_2 (titania) is the most appropriate metal oxide for photocatalytic processes due to its powerful oxidation and charge transport properties along with its abundance, nontoxicity, and stability to corrosion. It is promising in applications such as photogeneration of hydrogen from water, dye sensitized solar cells (DSSC), degradation of pollutants under visible light irradiation and production of hydrocarbon fuels.[1–4] Particularly, anatase phase has received an increased attention for it exhibits higher catalytic activity relative to rutile and brookite.[5] Intrinsic wide band gap of pure TiO_2 ($\sim$3.2 eV for anatase[6] and $\sim$3.0 eV for rutile[7]) confines its photon absorption to ultraviolet (UV) region severely limiting solar energy utilization to $\sim$5%. Great efforts have been made to modify the electronic properties of titania in order to extend its optical absorption edge into visible region and enhance its photoresponse. For this purpose, numerous studies have proposed doping of TiO_2 with substitutional cations and/or anions as an effective approach.[8–17]

Nitrogen doped titania is considered to be one of the most effective photocatalysts. Although it has been extensively studied by both experimental and theoretical methods,[18–27] proper description of midgap states is still desirable. For instance, Asahi *et al.*[18] concluded that N substitution for O causes a band gap narrowing due to mixing of 2*p* states of N and O. On the contrary, Irie *et al.*[19] have suggested that the visible-light response in N-doped titania may be due to N 2*p* states isolated above the valence band maximum (VBM). The nature of N-induced modifications to the electronic band structure depends on the doping content.[20,23] Then, another question relates to increasing charge trapping rate with increasing N-doping which is associated with a localized state below the CB.[24] Most of the theoretical studies failed to put forward the existence of such a trap level.

Sulphur is another effective dopant in modifying the electronic structure of titania. S can be substituted either at an O site as an anion or at a Ti site as a cation, depending on the incorporation techniques.[28–35] Both of them exhibit high photocatalytic activity under visible light.[33] Moreover, visible light absorbance increases with the atomic percentage of S-dopant.[31,32] A reliable explanation based on the effect of S 3*p* states on the electronic structure of TiO_2 is desirable.

Monodoped TiO_2 is usually inefficient for light harvesting. For instance, increasing concentration levels of transition metal doping, such as W incorporation, has detrimental effects on photogenerated charge carrier mobility.[36–38] Well localized isolated energy levels might act as electron-hole recombination centers reducing photocatalytic efficiency. To passivate such trap states, *n*-*p* type codoping with anion and cation pairs has been proposed.[11–13] Suitably chosen codopants not only narrow the band gap, but also serve to counteract the presence of recombination centers.[39–41] For this purpose, many experiments have recently focused on the additional substitution of W into N-doped titania and reported significant enhancement of catalytic activity under visible-light irradiation relative to monodoped reference systems.[42–46]

We used screened exchange hybrid DFT method for a proper description of the electronic structure of N, S, W, W/N and W/S doped anatase TiO_2. We attempt to analyze densities of states (DOS) in relation to visible light absorbance and charge carrier trapping, by comparing with experimental observations where explanations are still needed. We also discuss atomic structures, thermodynamical energetics and charge states of these ions substituted into the anatase lattice.

II. COMPUTATIONAL METHOD

The spin-polarized hybrid density functional theory calculations were carried out using the Vienna *ab-initio* simulation package (VASP).[47] Ionic cores and valence electrons were treated by projector-augmented waves (PAW) method.[48,49] Plane wave basis set was used to expand the wavefunctions up to a kinetic energy cutoff value of 400 eV. We used fine FFT grids with high precision settings throughout the calculations.

Standard DFT usually employs local or semilocal approximations to the exchange-correlation (XC) energy. This leads to erroneous descriptions for some real systems like transition metal oxides. One way of overcoming this deficiency is to use hybrid functionals, where a portion of the non-local Hartree-Fock (HF) type exchange is admixed with a semilocal XC functional. We used the Heyd-Scuseria-Ernzerhof hybrid functional (HSE06)[50–52] which adopts a screened Coulomb potential. Hence, the exchange hole becomes delocalized around a reference point but not beyond, reducing self-interaction error. Moreover, resulting rapid spatial decay of HF exchange improves the convergence behavior of self-consistent procedures. The HSE exchange is derived from the PBE0[53,54] exchange by range separation and then by elimination of counteracting long range contributions, as,

$$E_x^{\text{HSE}} = aE_x^{\text{HF,SR}}(\omega) + (1-a)E_x^{\text{PBE,SR}}(\omega) + E_x^{\text{PBE,LR}}(\omega),$$

where a is the mixing coefficient and ω is the range separation parameter. A consistent screening parameter of ω=0.2 Å^{-1} is used for the semilocal PBE exchange as well as for the screened non-local exchange as suggested for the HSE06 functional.[55] The choice of exact exchange contribution coefficient is important. Becke[56] derived a value of 20% by fitting to atomization energy data of a large number of molecular species. Later, it was suggested to be 25% by Perdew *et al.*[57] We adjusted this mixing to be 22% with which band gaps and lattice parameters for both anatase and rutile phases of titania can be obtained in good agreement with the experimental data as given in Table I.

We used a 108-atom supercell constructed by 3×3×1 replication of the anatase unit cell, which ensures sufficient spatial separation between the periodic images of the impurities as shown in Fig. 1. Various dopings of TiO_2 have been modeled by substitution of N (or S) at O and/or W at Ti sites. We also tried S@Ti configuration and found that this is energetically 1.246 eV/cell less favorable than S@O. For geometry optimizations and electronic structure calculations, the Brillouin zone was sampled with 2×2×2 mesh of special k-points. Previously, the same grid was shown to be sufficient to study oxygen vacancy formation in anatase TiO_2 using a smaller (76-atom) cell.[58] Atomic positions and cell parameters were fully optimized until spatial components of residual forces on each ion were below 0.015 eV/Å performing collinear spin polarized calculations.

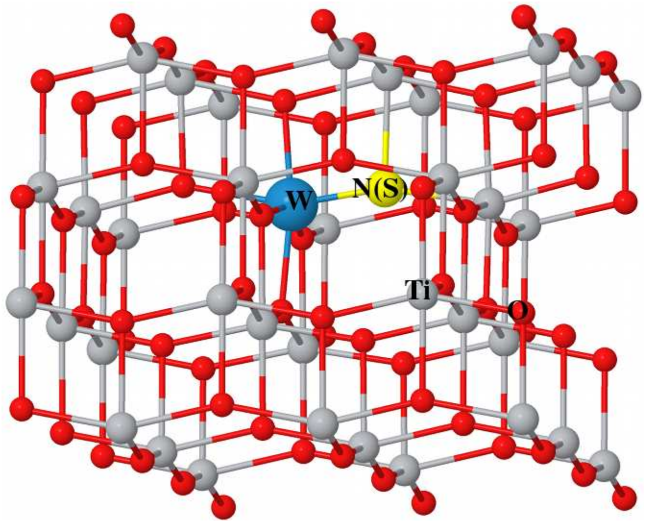

FIG. 1. Model bulk cell structure containing 108 atoms for W/N(S) (co)doped anatase TiO_2. Substitutional dopants are shown for N(S) at an O site, and for W at a Ti site.

We calculated (co)dopant formation energies using,

$$E_f = E_{\text{doped}} - E_{\text{pure}} - n\mu_{\text{W}} - m\mu_{\text{N(S)}} + n\mu_{\text{Ti}} + m\mu_{\text{O}},$$

where E_{doped} and E_{pure} are the total energies of doped and pure supercells, while μ_{W}, μ_{N}, μ_{S}, μ_{Ti} and μ_{O} are the chemical potentials of the W, N, S, Ti and O species, respectively. The integer n gives the number of W cations and m denotes the number of N(S) anions. In thermodynamical equilibrium with the anatase phase, μ_{Ti} and μ_{O} must satisfy the relation $\mu_{\text{TiO}_2} = \mu_{\text{Ti}} + 2\mu_{\text{O}}$. The amount of Ti and O in a growth environment influences their chemical potentials. High(low) values of μ_{O} correspond to O-rich(-poor) conditions and can also be interpreted as Ti-poor(-rich) conditions from the equilibrium relation. Under O-rich conditions, μ_{O} is the half of the energy of an O_2 molecule (E_{O_2}), and μ_{Ti} is obtained through the condition $\mu_{\text{Ti}} = \mu_{\text{TiO}_2} - E_{\text{O}_2}$. Under Ti-rich conditions, μ_{Ti} is the energy of a Ti atom in its bulk unit cell ($\mu_{\text{Ti}}^{\text{bulk}}$) and μ_{O} is calculated from the equilibrium restriction by $\mu_{\text{O}} = \frac{1}{2}(\mu_{\text{TiO}_2} - \mu_{\text{Ti}})$. The chemical potentials of the dopants are extracted from their naturally occurring phases. μ_{W} is calculated as $\mu_W = E_{\text{WO}_3} - \frac{3}{2}E_{\text{O}_2}$. Similarly, μ_{S} is obtained from the relation $\mu_S = E_{\text{SO}_2} - E_{\text{O}_2}$. For N, we used $\mu_{\text{N}} = \frac{1}{2}E_{\text{N}_2}$. Calculated dopant formation energies are given in Table II.

For the qualitative description of interatomic charge distributions, we used Bader analysis based on atom in molecule (AIM) theory. Local charge depletion/accumulation can be computed by integrating Bader volumes around atomic sites. These volumes are partitions of the real space cell delimited by local zero-flux surfaces of charge density gradient vector field. We calculated charge states of atomic species (see Table III) using a grid based decomposition algorithm developed by Henkelman's group.[59]

III. RESULTS & DISCUSSION

For the pure TiO_2, the calculated lattice parameters show remarkable agreement with the experimental data as presented in Table I. The calculated band gap values using the bulk unit cells for both anatase and rutile polymorphs are largely corrected by the HSE functional. When we use 108-atom supercell for the anatase case, it slightly changes to 3.23 eV as indicated in Fig. 4a. The bottom of the CB is formed by highly dispersing Ti $3d$. (see PDOS in Fig. 4g) They are not isolated but a part of the CB in consistency with the energy bands of pure anatase calculated with HSE06 by Yamamoto *et al.*.[16] Calculated Bader charges yield oxidation states of +2.84 and −1.43 for Ti and O, respectively. These are closer to formal values relative to those obtained by PBE.[60]

TABLE I. Computational results and experimental data (in parantheses) for the bulk material properties of TiO_2. Calculations were performed using the HSE06 functional with a 22% exact exchange contribution.

Phase	Lattice parameters		Transition	Band gap
	a (Å)	c (Å)		(eV)
Rutile	4.57 (4.59)[61]	2.94 (2.95)[61]	$\Gamma \to \Gamma$	2.97 (3.0)[7]
Anatase	3.78 (3.78)[61]	9.45 (9.50)[61]	$Z \to \Gamma$	3.20 (3.2)[6]

N@O doping : Substitution of single N atoms at O sites was confirmed by several reports.[18–21] Relaxed geometry of N dopant in the crystal has been shown in Fig 2. HSE functional gave a nearest neighbor Ti-N bond length of 1.96 Å while Ti-O bond was found to be 1.93 Å in its pure anatase phase. In addition, Ti-N bond along [001] is (2.07 Å) slightly larger than that of the Ti-O being 1.97 Å. Hence, N@O doping has a little effect on the lattice structure. Consistenly, the calculated charge states for N and O are $-1.38e$ and $-1.43e$, respectively. (see Table III) Hence, replacement of an O with an N is not expected to cause significant distortions in the lattice structure. In fact, N@O has the lowest formation energy, 0.53 eV, under O-poor conditions among all considered in this study. (Table II) When O is abundant in the environment it reasonably increases to 5.10 eV.

For the explanation of visible light response of N substituted TiO_2, the experiments (other than the study Irie *et al.*[19]) mainly agree on the band gap narrowing due to hybridization of N $2p$ and O $2p$ states.[18,21,22,24] This partial answer needs to be complemented with the possible presence of an impurity level below the CB as indicated by recombination characteristics of photogenerated electron-hole pairs[24] and variation of photoresponse under irradiation with different wavelengths.[19,22,23] Using X-ray photoelectron spectroscopy (XPS), Irie *et al.*[19] suggested an isolated N $2p$ narrow band formation above the VB, which is attributed to be responsible for the visible light sensitivity. Recently, deep-level optical spectroscopy (DLOS) measurements of Nakano *et al.* have located two deep levels at ∼1.18 and ∼2.48 eV below the CB.[21] The 2.48 eV band has been identified to behave as a part of the VB by mixing with the O $2p$ bands, which contributes to band gap narrowing. For the former, the possibility of oxygen vacancies depending on the processes involved in preparation of the samples were addressed as a potential origin of the impurity level closer to the CB.[21,22,24] However, this issue is still unclear. For instance, empty N orbitals might be involved.[23]

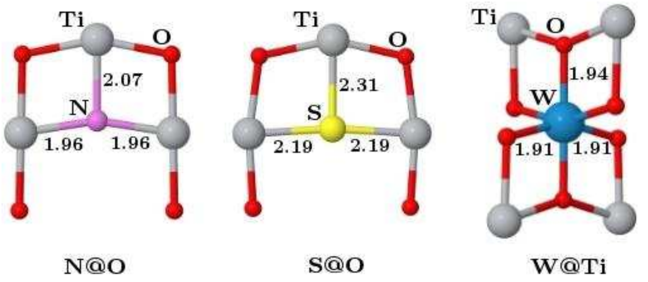

FIG. 2. Relaxed structures of monodopants, N, S and W inside anatase TiO_2 lattice. Bond lengths are in angstroms.

From the theoretical side, the position and the number of defect states in the band gap show differences depending on the type of DFT methods. For instance, local density approximation (LDA) predicts single N $2p$ state at the edge of VBM.[39] Generalized gradient approximation (GGA) and GGA+U studies predicted it to be isolated above the VBM.[26,27,40,41] In the DFT+U method, the supplementary on-site repulsion, U, acts only on Ti $3d$ electrons and is specific to the system under consideration. In this study, we identified two N driven gap states (in Fig. 4b,4h) based on the screened Coulomb potential approach. One of them is a singly occupied bonding state showing dominant N $2p$ character and is at the edge of VBM causing a considerable band gap narrowing by mixing with O $2p$ states. Moreover, PDOS reveals an increasing contribution of N toward the upper part of the VB. Consistenly, the presence of single-atom N impurities as diamagnetic (singly occupied) centers was previously observed in the electron paramagnetic resonance (EPR) studies.[22] The hybrid character of this state has been confirmed by many experiments.[18,21–24] This reflects a strong covalency of N centers with the TiO_2 matrix as shown in the ground state total electronic density in Fig. 5a. From diffuse reflectance spectroscopy (DRS) measurements, Spadavecchia *et al.*[23] reported an "apparent" band gap of 2.88 eV at 0.4 N/Ti molar ratio, which matches with our calculations as depicted in Fig. 4h. Similarly, Livraghi *et al.* found it to be 2.84 eV from their EPR spectra.[22]

Reports focusing on the charge carrier dynamics tend to offer the possibility of oxygen vacancy levels 0.75 – 1.18 eV below the CB.[21,24,25] Since reduction of the charge separation efficiency under visible light excitation is significantly large, vacancies are believed to promote recombination of holes and electrons. Our HSE calculations predicted an antibonding energy level for one spin component characterized dominantly by N $2p$ isolated 0.63 eV below the CB (see Fig. 4h). In the visible region, it might well act as a trap level centered at the N impurity site. The decrease in the quantum yields with increasing N concentration can also be associated to this empty N $2p$ energy level which does not conflict with possible existence of adjacent oxygen vacancies. Consistently, Spadavecchia *et al.*[23] opened up the possibility of charge transfer into empty N orbitals for the explanation of trapping mechanism.

S@O doping : Sulphur was shown to be incorporated into an O site of anatase lattice by oxidative annealing of TS_2.[28,29,32] Cationic doping was also achieved by Ohno *et al.*.[30] Recently, Li *et al.* reported an alternative synthesis procedure for S substitution for O.[33] We relaxed both S@O and S@Ti configurations on 108-atom supercell and found that the former is energetically more favorable by 1.246 eV/cell. Optimized geometry of a S dopant replacing the lattice O is depicted in Fig. 2. In comparison to an oxygen, the valence electrons of the S dopant have occupy more space. (see Fig. 5b) Therefore, the Ti-S bond lengths become 2.19 and 2.31 Å. while the corresponding Ti-O bonds are 1.93 and 1.97 Å in undoped anatase. These local structural changes cause an increase in the formation energy (in Table II) of an S dopant relative to that of N. The calculated value is 3.58 eV under O-poor conditions in reasonable agreement with a previous theoretical study.[35] However, the charge state of S(O) is calculated with HSE as $-1.17e(-1.43e)$ (in Table III) whereas it was previously predicted by pure DFT to be $-0.28e$ and $-0.67e$ for S and O, respectively.[35] Nominally S is expected to remain as S^{2-} similar to O^{2-} in the crystal. Briefly, the HSE functional improves the spatial distribution of charge densities and estimates electronegativities closer to the nominal values.

Furthermore, screened hybrid functional better describes the effects of the S anion on the electronic structure of TiO_2 where pure DFT fails. For instance, the PBE functional estimates a band gap narrowing of 0.45 eV at an S concentration of 0.0139 (one S atom in a 72-atom cell) after applying a scissors correction of 1.4 eV.[34] Our HSE calculations estimate the apparent band gap as 2.24 eV that corresponds to an effective narrowing of 0.99 eV for S@O doping in agreement with UV-vis diffuse reflectance spectra (DRS).[32,33] As seen in Fig. 4i, a group of hybrid states localized at the edge of the VB resulting from O $2p$, Ti $3d$ and dominantly S $3p$ coupling. This hybridization agrees well with the formation of S-Ti-O bonds as reported by Li *et al.* These hybrid states facilitate a state-to-band transition at 2.24 eV (~554 nm) might explain the observed absorbance edge at around 560 nm.[32,33] The increase in the visible DRS intensities with S concentration can be attributed to increased excitation probabilities by larger DOS contribution and extended dispersion of S-Ti-O states. In addition, the mixing of S $3p$ with O $2p$ band states increases VB width by 0.16 eV relative to the VBM of pure TiO_2. Similarly, overlap of antibonding S $3p$ orbitals with Ti $3d$ states decreases the CBM by 0.13 eV. These changes in the band edges allow band-to-band transitions starting from 2.94 eV (~422 nm) . This might be useful in explaining the redshift of absorbance shoulder near UV in DRS data.[28,32,33]

W@Ti doping : Experiments use sol-gel and microemulsion techniques to incorporate W into Ti sites.[36,38] Hence, oxygen is always present in the environment. In parallel, we calculated a moderate formation energy of 3.30 eV for W@Ti doping under O-rich conditions. (see Table II) On the other hand, when Ti is abundant, it gets as large as 12.45 eV. Substitution of W at Ti in the anatase lattice results in sixfold coordination as shown in Fig. 2. Four conjugate W-O bonds are 1.91 Å while the bonds along [001] direction become 1.94 Å. These are slightly shortened relative to those of the undoped TiO_2. In fact, the ionicity of W-O bonding is lower then a Ti-O bond as seen in Fig. 5c. In parallel, the Bader charges around W^{6+} and Ti^{4+} nominal species are found to be $-1.40e$ (W@Ti) and $-1.16e$ (Ti@pure), respectively. The disturbance on the lattice caused by the substitutional W is small and remains local. Although these values are lower than the formal charge states, partial inclusion of exact HF exchange improves them with respect to previous DFT results.[40]

In addition, W-doping causes formation of occupied states 0.25 eV below the CB with W $5d$ and Ti $3d$ contributions (Fig. 4d), which manifest similar DOS characteristics with an oxygen vacancy state[58,60] and also with those of Nb and Ta monodopings described by Ya-

TABLE II. Calculated formation energies (eV) for W, S, N, W/N, W/S doping of anatase supercell with 18 TiO_2 units.

	Ti-rich	O-rich
N-doped	0.53	5.10
W-doped	12.45	3.30
S-doped	3.58	8.16
W/N-doped	10.44	5.87
W/S-doped	15.81	11.23

TABLE III. Average charge states (e) of dopants and their adjecent Ti and O atoms from Bader analysis.

Dopant	N	S	W	Ti(nn)	O(nn)
none				+2.84	−1.43
N	−1.38			+2.31	
W			+4.60		−1.56
S		−1.17		+2.78	
W/N	−2.08		+4.76	+2.82	−1.53
W/S		−1.29	+4.20	+2.73	−1.54

mamoto *et al.*[16] Removal of an oxygen leaves excess electrons which accumulate around Ti ions. In a similar manner, W@Ti introduces excess electrons, a portion of them accumulating around the W center. (Fig. 5c) In fact, the oxidation states of W and Ti species in Table III reveal that the W valence shell $5d^4 6s^2$ loses 4.60 of its charge while Ti $3d^2 4s^2$ gives 2.84 of it to form bonds with adjacent oxygens. Therefore, the charge accumulation around the W center amounts to $1.40e$ being larger by $0.24e$ than that of Ti. Moreover, a very weak coupling between W and Ti d states can be seen in the PDOS analysis of these shallow states (Fig. 4j). The W $5d$ appears as a sharp dos peak for the majority spin component while Ti $3d$ contribution is broader involving both spins. The existence of impurity levels close to the CB was also discussed by experimenttal studies.[36,38] Yang *et al.* reported a red-shifted onset of optical absorption corresponding to an effective band gap of 2.73 eV for 3% W doping. In parallel, HSE predicts the defect states lying 2.81 eV above the VBM. Under visible light irradiation 19 at.% W-doped TiO_2 absorbs up to ∼445 nm (Fig.6 in Ref[[36]]) that is in good agreement with our estimation of 442 nm. Further, increasing W content reduces photocatalytic activity.[38] This can be ascribed to increased W $5d$ contribution on the defect states which can act as trap levels.

W/N codoping : In an attempt to address the charge recombination bottleneck observed in N-doped TiO_2, Gao *et al.* proposed an additional coupling to WO_3.[43] Numerous studies have shown drastic enhancement of the photocatalytic performance of titania based on passivation of the trapping mechanism by W-N codoping.[42–46]

We considered W and N in the 108-atom cell (Fig. 1) with different initial configurations, and found that the W-N pair shown in Fig. 3a(c) is the lowest energy structure. In agreement, Gao *et al.*[43] reported the generation of N–W–O linkage to be responsible for the increase in the visible light response. The interaction between W and N is much stronger with HSE, giving a bond length of 1.78 Å which is significantly shorter than the GGA+U estimation of 1.85 Å.[41] W-N pair imposes small local distortions while maintaining the optimal anatase structural properties as pointed out by Kubacka *et al.*[44]. For instance, T-N bond length being 2.00 Å is slightly longer than 1.96 Å of N@O case (in Fig 2). Supportingly, Kubacka *et al.* emphasized that W presence in anatase lattice is likely to influence the Ti-N bond. Moreover, screened hybrid functional predicts lower formation energy for W/N codoping compared with previous theoretical studies. For example, we calculated E_f as 5.87 eV under O-rich conditions. (Table II) It was estimated to be ∼8 eV by GGA+U method using a similar formulation.[41]

Electronically, both W@Ti and N@O cells resulted in magnetic ground states with spin multiplicities of 0.8 and 1.0, respectively. The energy of the W $5d$ donor level (in Fig 4j) is compatible with that of the N $2p$ acceptor level (in Fig 4h). Hence, pairing of W with N in the lattice forms $5d$–$2p$ hybridization giving zero net magnetic moment as seen in Fig 4k. This will, in turn, be effective in passivation of electron-hole recombination at dopant centers.

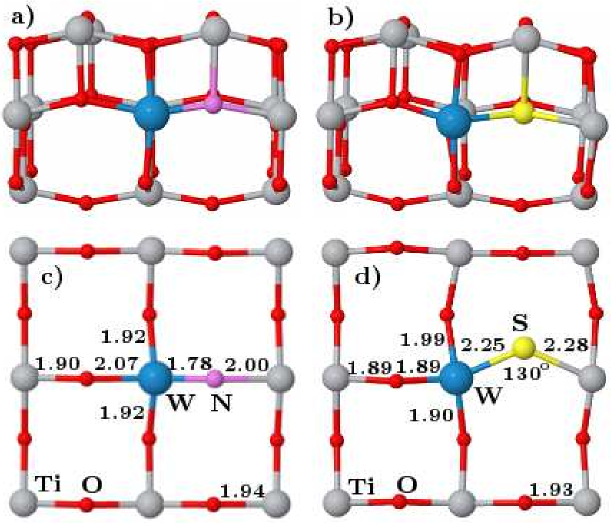

FIG. 3. Optimized atomic structures of W/N(S) codopants in anatase TiO_2. Side views (a),(b) through [010] and top views (c),(d) along [001] directions are presented for W/N and W/S, respectively.

Analysis of the Bader charges (in Table III) reveals that N gets oxidized more by $0.7e$ relative to N@O (see Fig.s 5a,d). This charge is partially transferred from the nearest neighbor W ($0.16e$ by comparing with W@Ti) A large part is taken from the adjacent Ti atom such that its stoichiometric charge state is almost restored (by comparing Ti oxidation states in pure, N@O and W/N cases). In the presence of W-N pair, the oxidation state of the adjacent Ti is +2.82 (in Table III). Briefly, the charge states of N and W get closer to formal oxidation values. This leads to a mutual passivation of N and W driven defect states. Indeed, the PDOS contribution of W $5d$ in the isolated states below the CB of W@Ti disappears by mixing with N $2p$ gap states. Therefore, W/N codoping causes formation of isolated defect states 0.18 eV below the CB characterized by Ti $3d$–N $2p$ bonding. Consequently, HSE predicts a weak metallization for this nonstoichiometric codoping.

When W codopant pairs with N, the position of N driven state at the VBM of N@O essentially remains the same. The main difference, however, is the disappearance of N $2p$ acceptor level of N@O. with the presence of W $5d$ donor level. The CB edge shows similar characteristics with that of W@Ti. In Fig. 4k, Ti $3d$–N $2p$ defect states lie 2.65 eV above the VB. This corresponds to an effective reduction of the band gap by 0.58 eV with respect to that of pure anatase. In previous experimental studies this narrowing was reported to be 0.55 eV.[44–46] However, pure GGA and GGA+U studies found 0.2 and 1.11 eV gap narrowing values.[40,41] Partial compensation of deficient charge by W/N pairing was also confirmed to improve the photocatalytic efficiency supporting our results.[42–46]

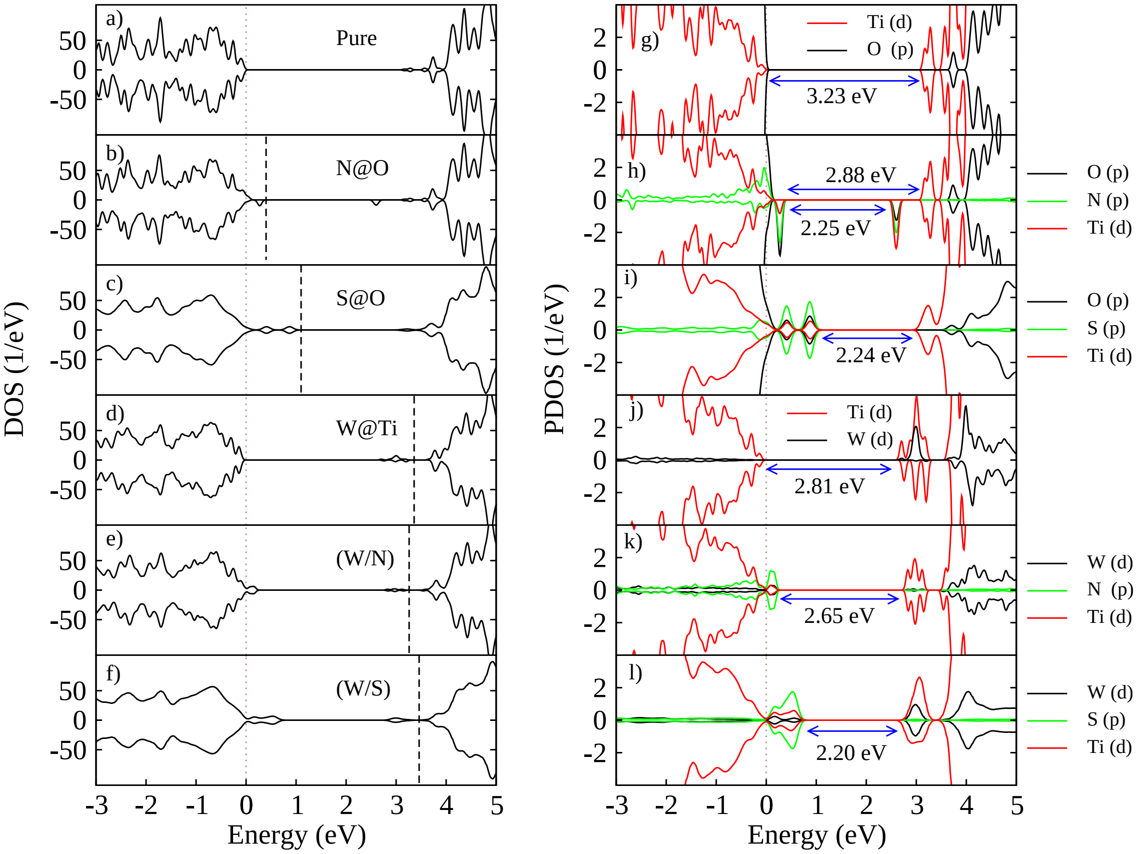

FIG. 4. Total (left pane) and projected (right pane) densities of states (DOS) of pure and, W and/or N(S) substituted anatase TiO_2, calculated with HSE06 functional. Dashed lines indicate the Fermi energies. Dotted line denote the VBM of pure TiO_2.

W/S codoping : Monodoping of both S and W has been experimentally achieved to be effective in increasing the optical absorption efficiencies of TiO_2, suggesting the possibility of W/S codoping. This so that presence of S modifies the VB edge and brings defect states at the VBM by mixing with O $2p$ and Ti $3d$ band states. In addition, shifting of the CBM and the $5d$ donor levels are induced by W substitution. Therefore, as in the case of W/N, coexistence of S and W species is expected to have a cooperative effect on band gap narrowing. Guided with this reasoning, we investigated the lowest energy configuration of W and S substituted 108-atom anatase cell and found that W-S pairing as shown in Fig. 3b,d is energetically more favorable than other possibilities. For instance, relaxed geometry of non-pairing W-O-S configuration is 3.62 eV/cell higher in energy. W-S pair noticeably distorts the lattice relative to W/N case. However, the effect of this distortion remains local. The coordination of S with W and Ti increases W-S and Ti-S bond lengths. In fact, Ti-S bond being 2.19 Å in S@O gets slightly larger by 0.09 Å by additional substitution of a W as shown in Fig. 3d. Since relatively large W-S (2.25 Å) and Ti-S (2.28 Å) bonds do not fit in the anatase network, S atom relaxes out of the lattice site. This distortion results in increased formation energies with respect to those of W/N codoping as presented in Table II, which suggests synthesis under O-rich conditions is more probable similar to the W/N.

Bader analysis reveals that S codopant gets more oxidized ($-1.29e$) with respect to S@O case ($-1.17e$). The charge states of the W ($+4.20e$) and of the adjacent Ti ($+2.73e$) indicate slightly less electron depletion from around them, particularly, relative to the W/N case. Passivative codoping effects of the corresponding charge transfers can be seen in the DOS structures of the W/S system in Fig.s 4f and 4l. For instance, as a result of W $5d$–S $3p$ hybridization, the PDOS peak of the W gets broadened inside the defect states relative to that of the W@Ti case. In fact, these states form as a result of the mixing of W $5d$–S $3p$–Ti $3d$ bonding states with largely dispersing Ti $3d$ CB bands. As in the W-doped and the W/N cases, the Fermi energy is pinned above the W $5d$ donor level similar to an oxygen vacancy situation.[58,60] Hybridization of orbitals is not limited to these defect states at the CBM. S $3p$ orbitals also mix with the VB continuum. Moreoever, a group of largely dispersing hybrid states (dominantly driven by S $3p$ orbitals) form as a part of the VB edge. The shift of the VBM into higher energies is similar to the S monodoping case. This results in an effective band gap narrowing of 1.03 eV which is

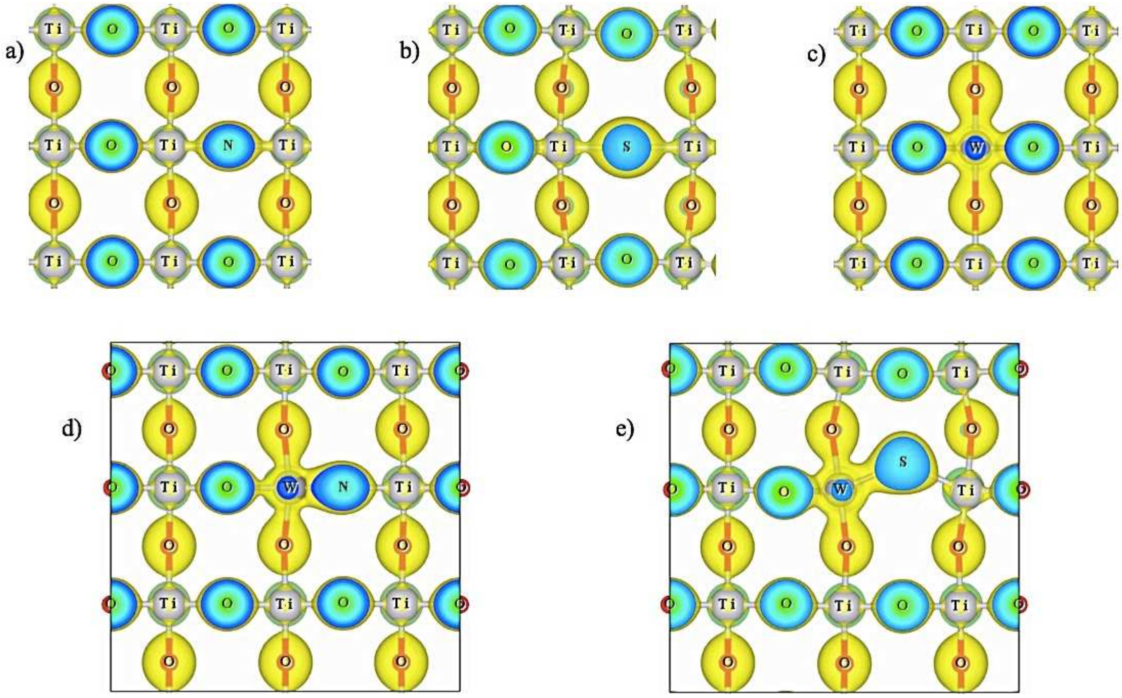

FIG. 5. Ground state total charge densities of (a) N-, (b) S-, (c) W-monodoped and (d) W/N-, (e) W/S-codoped anatase TiO_2. These 3D plots have been cut through (001) plane slightly above the dopant species for visual convenience.

much larger than that of the W/N codoping. The apparent band gap value becomes 2.20 eV allowing optical absorption up to $\sim$564 nm. Partial passivation of W 5*d* trap levels by S pairing might reduce electron-hole recombination rate. Also, W 5*d* states are more delocalized relative to typical 3*d* or 4*d* orbitals and they strongly couple to the CB of TiO_2 which might help passivate the carrier recombination. Since impurity derived states at the VBM and CBM are fully occupied, interband transitions are much more effective than localized state-to-band transitions, due to a much larger intensity. Narrowing band gaps without creating isolated states are much more effective for photocatalytic activity.[13,39] In this sense, W/S codoping is predicted to drastically redshift the visible light absorption onset involving strong band-to-band and also band-to-state transitions, which, in turn, enhances the photocalaytic efficiencies.

IV. CONCLUSIONS

We have systematically analyzed the atomic and electronic structures of N, S, W, W/N and W/S doping in anatase TiO_2 by the screened Coulomb potential approach. Our HSE results can be useful in explaining optical absorption spectra of these systems evidenced by many experiments. In this way, for the N doped-TiO_2, we identified an N 2*p*–O 2*p* hiybrid state at the VBM and an N 2*p* unoccupied trap level isolated 0.63 eV below the CB. This might serve as an alternative explanation to solve some of the controversial experiment findings. Similarly, we are able to offer an understanding of the increased photocatalytic efficiencies observed for W/N codoping. The pair mixing of N 2*p* orbitals with the isolated W 5*d* levels has been shown on the basis of their DOS structures. W–N pairing results in a band gap narrowing of 0.58 eV. As a trend, our HSE calculations might be useful in the interpretation of the passivative effect of such a pairing of a non-metal with a d-band metal. Then, we examined W/S codoping in anatase. By comparing modifications in the DOS structures we predict the origin of redshifts in the absorption light edge with W/N and W/S codoping systems. In fact, W/S codoping significantly reduces the optical absorption treshold which allows light harvesting in the large part of the visible range. Therefore, codoping of anatase TiO_2 with W and S is expected to achieve highly efficienct photocatalysis because the low lying photo-excitations involve transitions from S 3*p* to Ti 3*d* and W 5*d* bands through an energy difference of 2.20 eV and the positons of these states are compatible with the redox potentials of water.

ACKNOWLEDGMENTS

We acknowledge partial support from TÜBİTAK, The Scientific and Technological Research Council of Turkey (Grant No. 110T394). Computational resources were provided by ULAKBİM, Turkish Academic Network & Information Center.

---

[1] A. Fujishima, K. Honda, Nature (London) **238**, 37 (1972).

[2] M. Grätzel, Nature (London) **414**, 338 (2001).

[3] S. U. M. Khan, M. Al-Shahry, W. B. Ingler, Jr., Science **297**, 2243 (2002).

[4] O. K. Varghese, M. Paulose, T. J. LaTempa, C. A. Grimes, Nano Lett. **9**, 731 (2009).

[5] M. Xu, Y. Gao, E. M. Moreno, M. Kunst, M. Muhler, Y. Wang, H. Idriss, C. Wöll, Phys. Rev. Lett. **106**, 138302 (2011).

[6] H. Tang, H. Berger, P. E. Schmid, F. Levy, G. Burri, Solid State Commun. **87**, 847 (1993).

[7] J. Pascaul, J. Camassel, H. Mathieu, Phys. Rev. Lett. **37**, 1490 (1977), Phys. Rev. B **18**, 5606 (1978).

[8] W. Mu, J. M. Herrmann, P. Pichat, Catal. Lett., **3**, 73 (1989).

[9] W. Choi, A. Termin, M. R. Hoffmann, J. Phys. Chem. **98**, 13669 (1994).

[10] S. Sakthivel and H. Kisch, Angew. Chem., Int. Ed. **42**, 4908 (2003).

[11] H. Sun, Y. Bai, Y. Cheng, W. Jin, N. Xu, Ind. Eng. Chem. Res. **45**, 4971, (2006).

[12] P. Wang, Z. Liu, F. Lin, G. Zhou, J. Wu, W. Duan, B.-L. Gu, S. B. Zhang, Phys. Rev. B **82**, 193103 (2010).

[13] H. Yu, H. Irie, and K. Hashimoto, J. Am. Chem. Soc. **132**, 6898 (2010).

[14] W. Zhu, X. Qiu, V. Iancu, X.-Q. Chen, H. Pan, W. Wang, N. M. Dimitrijevic, T. Rajh, H. M. Meyer, M. P. Paranthaman, G. M. Stocks, H. H. Weitering, B. Gu, G. Eres, Z. Zhang, Phys. Rev. Lett. **103**, 226401 (2009).

[15] R. Long, N. J. English, Phys. Rev. B **83**, 155209 (2011).

[16] T. Yamamoto, T. Ohno, Phys. Rev. B **85**, 033104 (2012).

[17] W.-J. Yin, S.-H. Wei, M. M. Al-Jassim, Y. Yan, Phys. Rev. Lett. **106**, 066801 (2011).

[18] R. Asahi, T. Morikawa, T. Ohwaki, K. Aoki, Y. Taga, Science **293**, 269 (2001).

[19] H. Irie, Y. Watanabe, K. Hashimoto, J. Phys. Chem. B **107**, 5483 (2003).

[20] J.L. Gole, J.D. Stout, C. Burda, Y. Lou, X. Chen, J. Phys. Chem. B **108** 1230-1240 (2004).

[21] Y. Nakano, T. Morikawa, T. Ohwaki, Y. Taga, Appl. Phys. Lett. **86**, 132104 (2005).

[22] S. Livraghi, M. C. Paganini, E. Giamello, A. Selloni, C. Di Valentin, G. Pacchioni, J. Am. Chem. Soc. **128**, 15666 (2006).

[23] F. Spadavecchia, G. Cappelletti, S. Ardizzone, M. Ceotto, L. Falciola, J. Phys. Chem. C **115**, 6381 (2011).

[24] R. Katoh, A. Furube, K. Yamanaka, and T. Morikawa, J. Phys. Chem. Lett. **1**, 3261 (2010).

[25] K. Yamanaka, T. Morikawa, J. Phys. Chem C **116**, 1286 (2012).

[26] J. G. Tao, L. X. Guan, J. S. Pan, C. H. A. Huan, L. Wang, J. L. Kuo, Z. Zhang, J. W. Chai, S. J. Wang, Appl. Phys. Lett. **95**, 062505 (2009).

[27] M. Harb, P. Sautet, P. Raybaud, J. Phys. Chem. C **115**, 19394 (2011).

[28] T. Umebayashi, T. Yamaki, H. Itoh, K. Asai, Appl. Phys. Lett., **81**,454, (2002).

[29] T. Umebayashi, T. Yamaki, S. Tanaka, K. Asai, Chem. Lett., **32**, 330, (2003).

[30] T. Ohno, M. Akiyoshi, T. Umebayashi, K. Asai, T. Mitsui, M. Matsumura, Appl. Catal., A, **265**, 115, (2004).

[31] J. C. Yu, W. Ho, J. Yu, H. Yip, P. K. Wong, J. Zhao, Environ. Sci. Technol., **39**, 1175, (2005).

[32] W. Ho, J. C. Yu, S. J. Lee, Solid. State Chem., **179**, 1171, (2006).

[33] H. Li, X. Zhang,Y. Huo, J. Zhu, Environ. Sci. Technol., **41**, 4410, (2007).

[34] F. H. Tian, C. B. Liu, J. Phys. Chem. b **110**, 17866 (2006).

[35] K. Yang, Y. Dai and B. Huang, J. Phys. Chem. C, **111**, 18985-18994, (2007)

[36] A. Fuerte, M. D. Hernandez-Alonso, A. J. Maira, A. Martinez-Arias, M. Fernandez-Garcia, J. C. Conesa, J. Soria, G. Munuera, J. Catal. **212**, 1 (2002).

[37] N. Couselo, F. S. G. Einschlag, R. J. Candal, M. Jobbágy, J. Phys. Chem. C **112**, 1094 (2008).

[38] Y. Yang, H. Wang, X. Li, and C. Wang, Mater. Lett. **63**, 331 (2009).

[39] Y. Q. Gai, J. B. Li, A. S. Li, J. B. Xia, and S. H. Wei, Phys. Rev. Lett. **102**, 036402 (2009).

[40] R. Long, N J. English, Appl. Phys. Lett. **94**, 132102 (2009).

[41] R. Long, N. J. English, Chem. Mater. **22**, 1616 (2010).

[42] Y. Shen, T. Xiong, T. Li, K. Yang, Appl. Catal. B: Envir. **83**, 177, (2008).

[43] B. Gao, Y. Ma, Y. Cao, W. Yang, and J. Yao, J. Phys. Chem. B, **110**, 14391 (2006).

[44] A. Kubacka, B. Bachiller-Baeza, G. Colón, M. Fernandez-García, J. Phys. Chem. C,**113**, 8553 (2009).

[45] A. Kubacka, B. Bachiller-Baeza, G. Colón, M. Fernandez-García, Appl. Catal. B: Envir. **93**, 274, (2010).

[46] A. Kubacka, G. Colon, M. Fernandez-García, Appl. Catal. B: Envir. **95**, 238-244, (2010).

[47] G. Kresse, J. Hafner, Phys. Rev. B, **47**, 558 (1993).

[48] P. E. Blöchl, Phys. Rev. B **50**, 17953 (1994).

[49] G. Kresse, J. Joubert, Phys. Rev. B **59**, 1758 (1999).

[50] J. Heyd, G. E. Scuseria, M. Ernzerhof, J. Chem. Phys. **118**, 8207 (2003).

[51] J. Heyd, G. E. Scuseria, M. Ernzerhof, J. Chem. Phys. **124**, 219906 (2006).

[52] J. Paier, M. Marsman, K. Hummer, G. Kress, I. C. Gerber, J. G. Angyan, J. Chem. Phys. **125**, 249901 (2006).

[53] J. P. Perdew, K. Burke, M. Ernzerhof, Phys. Rev. Lett. **77**, 3865 (1996), Phys. Rev. Lett. **78**, 1396 (1997).

[54] C. Adamo, V. Barone, J. Chem. Phys. **110**, 6158 (1999).

[55] A. V. Krukau, O. A. Vydrov, A. F. Izmaylov, G. E. Scuseria, J. Chem. Phys. **125**, 224106 (2006).

[56] A. D. Becke, J. Chem. Phys. **98**, 1372 (1993); **99**, 5648 (1993).

[57] J. P. Perdew, M. Ernzerhof, K. Burke, J. Chem. Phys. **105**, 9982 (1996).

[58] A. Janotti, J. B. Varley, P. Rinke, N. Umezawa, G. Kresse, C. G. Van de Walle, Phys. Rev. B **81**, 085212, (2010).

[59] W. Tang, E. Sanville, and G. Henkelman, J. Phys.: Condens. Matter **21**, 084204 (2009).

[60] E. Mete, D. Uner, O. Gulseren, Ş. Ellialtıoğlu, Phys. Rev. B **79**, 125418 (2009).

[61] J. K. Burdett, T. Hughbanks, G. J. Miller, J. W. Richardson, Jr., J. V. Smith, J. Am. Chem. Soc. **109**, 3639 (1987).